where

$$I(V) = \ln(\tfrac{1}{2}V^2 + bV - a) + \frac{b}{(b^2+2a)^{1/2}} \ln\left[\frac{V+b+(b^2+2a)^{1/2}}{V+b-(b^2+2a)^{1/2}}\right] \quad (18)$$

and

$$V_m = 1/(\tau^{*1/2}). \quad (19)$$

4. DISCUSSION

The most important approximation used in the present derivation is the assumption that the liquid temperature distribution governed by convective cooling at time of freezing can be replaced by the temperature profile obtained using an isothermal boundary at $t = t^*$. t^* is obtained such that the liquid temperature gradient at the surface remains the same. Thus, the initial rate of solidification will not be affected. To examine the validity of the assumption used, the two liquid temperature profiles are compared. This is shown in Fig. 2 for $Ste' = 0.05012$ and $Ste = 0.01253$ and 0.1253. For water, this corresponds to $T_0 = 4°C$ and $T_a = -2°C$ and $-20°C$, respectively. The actual or convectively cooled profiles are obtained from equation (1) with $t = t_m$. The isothermally cooled profiles are given by [1]

$$\frac{T_i(y,t^*) - T_m}{T_0 - T_m} = \text{erf}\,\frac{y}{2(\alpha_i t^*)^{1/2}}. \quad (20)$$

It can be seen that the corresponding temperature profiles compare very well with each other. Thus, the use of the profile obtained using an isothermal boundary at t^* to replace the actual temperature profile at t_m is indeed a good approximation and its effect on surface freezing rate is expected to be small in general.

Typical results obtained by using the present approximate solution [i.e. equation (17)] are plotted in Fig. 3 for $Ste' = 0.05012$. Four Stefan numbers, $Ste = 0.01253$, 0.031325, 0.06265 and 0.1253, are used. This corresponds to $T_a = -2°C$, $-5°C$, $-10°C$ and $-20°C$ respectively for water. The freezing times (τ_m) for the curves were obtained using equation (1) with $T_i(y = 0) = T_m$ and $y = 0$.

As expected, the results show that the freezing rate increases rapidly as Ste increases, i.e. with lower ambient temperatures. Physically, the Stefan number is the ratio of the driving force for freezing and the resistance to freezing. Thus, higher Stefan numbers result in faster rates of freezing.

Also shown in Fig. 3 are results obtained numerically. The numerical results were obtained using as many as 160 grid points for accuracy. Details of the numerical procedure can be found elsewhere [8]. It can be seen that the analytical and numerical results compare very well, especially for higher Stefan numbers. For lower Stefan numbers, the analytical solution predicts freezing rates slightly lower than the numerical solution.

It should also be noted that: (i) the approximate solution obtained [equation (17)] is in dimensionless form. Therefore, the results shown in Fig. 3 are applicable for different phase change media and under different sets of boundary and initial conditions; (ii) for the special case with $T_0 \to T_m$, the present solution reduces identically to Foss's solution [8].

REFERENCES

1. H. S. Carslaw and J. C. Jaeger, *Conduction of Heat in Solids* (2nd edn.), pp. 282–296. Clarendon Press, Oxford (1959).
2. F. Jackson, The solution of problems involving the melting and freezing of finite slabs by a method due to Portnov, *Proc. Edinb. Math. Soc.* **14**, 109–128 (1964).
3. D. Langford, New analytical solutions of the one-dimensional heat equation for temperature and heat flow rate both prescribed at the same fixed boundary (with application to the phase change problem), *Q. Appl. Math.* **24**, 315–322 (1966).
4. B. Boley, A general starting solution for melting and solidifying slabs, *Int. J. Engng Sci.* **6**, 89–111 (1968).
5. K. O. Westphal, Series solution of freezing problem with the fixed surface radiating into a medium of arbitrary varying temperatures, *Int. J. Heat Mass Transfer* **10**, 195–205 (1967).
6. S. D. Foss, An approximate solution to the moving boundary problem associated with the freezing and melting of lake ice, *A.I.Ch.E. Symp. Ser.* **74** (174), 250–255 (1978).
7. P. J. Schneider, *Conduction Heat Transfer*. Addison-Wesley, Cambridge (1955).
8. A. M. C. Chan and M. Shoukri, On the analysis of water cooling and freezing in the CANDU vacuum building due to environmental conditions, Ontario Hydro Research Division Report (1983).

Int. J. Heat Mass Transfer. Vol. 26, No. 11, pp. 1715–1717, 1983
Printed in Great Britain

0017-9310/83 $3.00 + 0.00

OPTICAL ILLUSTRATION OF LIQUID PENETRATION TO THE VAPOUR FILM IN INVERTED ANNULAR BOILING

Z. EDELMAN, E. ELIAS and D. NAOT

Department of Nuclear Engineering, Israel Institute of Technology, Technion City, Haifa 3200, Israel

(*Received* 6 *August* 1982 *and in final form* 3 *March* 1983)

1. INTRODUCTION

INVERTED annular film boiling is an important stage in the reflooding phase of a loss-of-coolant accident (LOCA) in light water reactors. Heat transfer coefficients for inverted annular flow of water in a single vertical tube have been measured in steady-state experiments [1] and for more realistic flow conditions [2–4]. Seban *et al.* [5] and Edelman [4] have examined the experimental results in the region immediately downstream of the quench front for cases in which the water in this region was subcooled or had a very low quality and suggested that existing models for film boiling are inadequate for the specification of the heat transfer coefficient. Unfortunately models based on laminar [6] or turbulent [7] vapour boundary layers underpredict both the heat transfer coefficient and the vapour film thickness in the inverted annular region, as they neglect the vapour inlet velocity at the quench front, assuming that all the vapour is generated at the liquid interphase which is considered to be saturated. A

theoretical model based on an analytical solution of the energy equations in the vapour and liquid regions has been recently developed by Elias and Chambre [8]. Here the vapour film thickness depends on the fluid conditions at the quench front. The vapour film thickness was correlated using the steady-state results of Fung *et al.* [1]. While a good agreement with the experimental results was achieved for the low inlet velocity and low subcooling tests, the model predicts unrealistically high vapour velocities for the high inlet mass flux and subcooling experiments. These trends suggested the existence of heat transfer augmentation processes in the inverted annular region not considered by the model. Indeed, observations of such augmentation mechanisms were reported by several investigators [9–11]. Photographs of inverted annular flow above a quench front in a heated quartz tube obtained by Goodman and Elias [12] showed that the liquid core is not centrally positioned in the tube but, rather, fluctuates eccentrically imposing oscillations in the vapour film thickness.

Attempts to use temperature trajectories measured with thermocouples in a stainless steel tube in order to detect the liquid penetration into the annular vapour film in the inverted annular boiling, reported in ref. [4], raised doubts as to whether the signal sought can be effectively identified. A need for direct evidence became apparent. The present work is aimed to show the liquid penetration into the annular vapour film using optical means. Unfortunately, by using a quartz tube, the conditions such as temperature gradients and heat fluxes are not the same as those measured in the stainless steel tube and the illustration is restricted.

2. LIQUID PENETRATION TO THE VAPOUR FILM

The experimental set-up shown in Fig. 1 consisted of a long quartz tube (12 mm I.D. × 1200 mm long and 1.5 mm wall thickness). The tube was heated externally by approximately 100 small gas burners distributed on two sides along the tube. This configuration allows initial uniform heating of the tube at 600°C with a maximum axial temperature gradient of 1°C cm^{-1}. Water was pumped at a predetermined temperature of 21°C and flow rate to the bottom of the heated tube. The stability of the vapour film above the quench front was measured by a laser transmission technique. The system consisted of a narrow He–Ne laser beam (0.5 mm) traversing the test section horizontally, i.e. perpendicular to its axis. The beam was positioned such that it 'views' the vapour film region at the inner surface of the tube. The intensity of the transmittal beam was detected by a photoelectric cell with a short response time (33 ns). The effect of the infra-red light from the heating

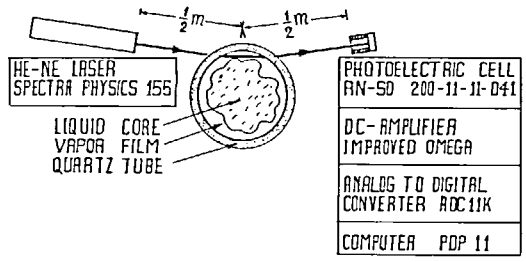

FIG. 2. The laser beam system.

burners was minimized by adequate collimation and positioning of the photoelectric cell. The system shown in Fig. 2 was calibrated before heating using four Plexiglas well centred cylinders to enable a quantitative determination of the instantaneous vapour film thickness within the 0.5 mm range.

Establishing an inverted annular boiling regime became possible due to operation with a low inlet equilibrium quality of −0.14 and a high inlet velocity of 17 cm s^{-1}. The first feature is smaller than −0.05 and the second is larger than the 7.5 cm s^{-1} recommended in ref. [4] for the limits of feasibility. Experience with the stainless steel tube, where heat balance could be performed, suggests that the equilibrium quality at the quench front remains lower than the −0.05 limiting value at the measurement cross section, and that the quench front velocity is reduced by less than 10% during the time period considered here.

Figure 3 shows a typical plot of the photoelectric cell response as a function of the distance from the quench front $Z-Z_{qf}$, for an inlet mass flux of 170 kg m^{-2} s^{-1} and an apparently constant quench front velocity of 6 cm s^{-1}. As the photoelectric response is proportional to the fraction of the beam cross section not covered by the fluid, i.e. transparent, it is referred to in Fig. 3 as the vapour fraction:

$$V_f = \frac{\text{Transparent area occupied by vapour}}{\text{Total area of the laser beam}}. \quad (1)$$

The 100% reading corresponds to the film thickness greater than the beam width (0.5 mm).

High film thickness conditions prevail in the beginning of the measurement far from the quench front (34 cm). As the quench front approaches the laser beam position, one observes rapid and intensive fluid penetrations to the vapour film until finally the wall is wetted (quench front) and the beam is shifted completely from the detector. The objective of the

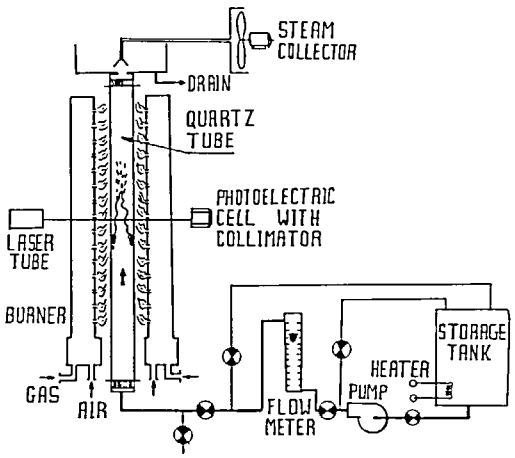

FIG. 1. The quartz tube system.

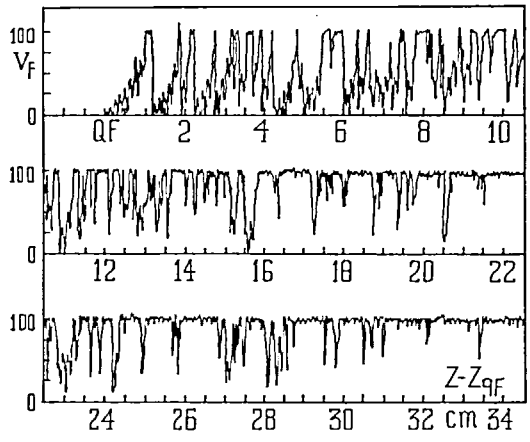

FIG. 3. Vapour fraction in the laser beam as a function of the distance from the quench front.

present illustration is to note that occasionally the laser beam is blocked almost completely by liquid, presumably due to attempts to wet the wall. This phenomenon is most effective near the quench front but is observed up to 30 cm downstream. It should be noted that at the measurement cross section (mid-tube) the length of the water column rising above the quench front before breaking completely into a dispersed flow is much larger than this distance. With a longer tube it may reach 1 m. The phenomena is typical of the region close to the quench front.

Figure 4 describes the distribution function and the differential frequency of the liquid fraction defined by

$$L_f = 1 - V_f. \tag{2}$$

The distribution function shown in Fig. 4(a) describes the probability that the liquid fraction L_f is greater than a specified value L_F

$$F = P(L_f \geqslant L_F), \tag{3}$$

as a function of the distance from the quench front. The frequency function shown in Fig. 4(b) describes the probability that the liquid fraction L_f is within the small margin Δ around a specified value L_F

$$f = \frac{1}{\Delta} P\left(L_F - \frac{\Delta}{2} < L_f < L_F + \frac{\Delta}{2}\right), \tag{4}$$

and is also given as a function of the distance from the quench front. Obviously the two are related by

$$f = -\partial F / \partial L_F, \tag{5}$$

and therefore f can be derived from F.

The number of measurements taken within the period of time sampled (1 s) was limited and therefore the data was used to correlate the distribution function (integral information). The dots in Fig. 4(a) which show the experimental data are expected to represent the centre of a 15% error margin. The lines fitted in Fig. 4(a) were then derived to produce the lines given in Fig. 4(b). Figure 4(b) suggests that the most frequent fluid penetrations manage to cover the whole beam (0.5 mm) near the quench front at a distance smaller than 8 cm. The most frequent fluid penetrations cover less than 30% of the beam at a distance from the quench front greater than 20 cm. Figure 4(a) suggests that the probability that at least half of the beam is covered by fluid is about 85, 70, 30, 20 and 3% for the distances of 2, 8, 14, 20 and 32 cm, respectively, from the quench front.

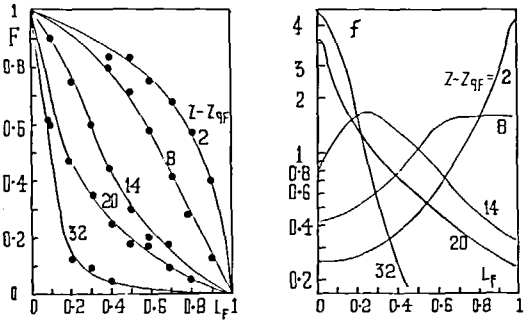

FIG. 4. Statistics of the liquid fraction in the laser beam (a) distribution function, (b) frequency function.

3. REMARKS

Although no conclusive observation can be derived from the data on whether the beam blocking stems from small droplets carried by the vapour from the liquid core or from the quench front region, roughness of the liquid–vapour interface, or a combination of these mechanisms, the overall effect is a reduced vapour layer thickness and an enhanced heat transfer from the wall. It is believed that modelling the heat transfer augmentation due to the fluctuations in the thickness of the vapour layer is required for a realistic prediction of the high heat fluxes observed in the inverted annular film boiling region.

To study the periodicity of the fluid penetration we need a Fourier analysis. It seems that the conditions vary with the distance from the quench front too fast to allow analysis for periods long enough for meaningful results. Still, to illustrate the periodicity one can observe in Fig. 3 a series of repeated patterns during the first 6 cm (1 s). Each basic pattern contains small oscillations superimposed on a single relatively larger pulse. Roughly we can observe a 50 Hz signal imposed on a basic 8 Hz signal. Following Fig. 3 in a reversed direction towards the quench front end of the graph we get the impression that we witness dramatically fast dry-out processes that follow nonstable and wavy rewetting processes. The quench front is the last attempt in the rewetting and dry-out series with no further dry-out. In terms of heat transfer augmentation it seems that the 8 Hz signal represents a series of small steam explosions where the liquid content of the whole layer is ejected due to fast evaporation.

REFERENCES

1. K. K. Fung *et al.*, *Nucl. Engng Des.* **55**, 51 (1979).
2. R. Seban *et al.*, EPRI Report NP-743 (1978).
3. D. Abdollahian, Ph.D. Thesis, University of California, Berkeley (1979).
4. Z. Edelman, Ph.D. Thesis (in Hebrew), Technion, Haifa, Israel (1981).
5. R. Seban *et al.*, EPRI Report NP-1290 (1979).
6. L. A. Bromley, *Chem. Engng Prog.* **46**, 221–227 (1950).
7. R. S. Dougall and W. M. Rohsenow, MIT Report 9079-26 (1963).
8. E. Elias and P. Chambre, *Nucl. Engng Des.* **69**, 249–257 (1981).
9. Y. Y. Hsu and J. W. Westwater, *Chem. Engng Prog.* **56**, 15 (1960).
10. G. E. Coury and A. E. Dukler, *Proc. Int. Heat Transfer Conf.*, Paper B.3.6, Paris (1970).
11. N. V. Suryanarayana and H. Merte, *Trans. Am. Soc. Mech. Engrs*, Series C, *J. Heat Transfer* **94**, 377–384 (1972).
12. J. Goodman and E. Elias, *Trans. Am. Nucl. Soc.* **28**, 397–399 (1978).